

ARTICLE TYPE

Cite this: DOI: 00.0000/xxxxxxxxxx

Depletion-induced crystallization of anisotropic triblock colloids[†]

Supplementary Information

Fabrizio Camerin,^{a,b*} Susana Marín-Aguilar,^{a*} and Marjolein Dijkstra^{a,b}

1 Simulation parameters

We present the experimental values for the inverse Debye screening length κ , the Bjerrum length λ_B , and the zeta potential for PS and TPM, ψ_{PS} and ψ_{TPM} , respectively, along with their conversions to simulation units in Table S1.

Parameter	Experimental units	Simulation units
κ	0.4 nm^{-1}	$114.57\sigma^{-1}$
λ_B	0.71 nm	$2.5 \times 10^{-3}\sigma$
ψ_{PS}	-15 mV	$-0.58k_BT/e$
ψ_{TPM}	-35 mV	$-1.36k_BT/e$

Table S1 Parameters used in the Yukawa potential (see Eq. 1 in the main text) for the two types of materials, PS and TPM, in experimental units retrieved from Ref. 1 and converted to simulation units: κ the inverse Debye screening length, λ_B the Bjerrum length, ψ_{PS} the zeta potential of polystyrene (PS) located at the tips of the triblock colloid and ψ_{TPM} the zeta potential of 3-(trimethoxysilyl)propyl methacrylate (TPM) located at the center of the triblock colloids.

2 Crystal Phase Characterization

To characterize the different crystalline phases, we compute the second Legendre polynomial (slp), and n -atic bond order parameters $\tilde{\Psi}_n$, with $n = 4, 6, 8$, of each identified crystal phase. These order parameters are also used as input for the Principal Component Analysis (PCA) used to identify the phases in the self-assembly simulations. They are calculated from configurations of fully crystalline systems of triblock colloids with varying aspect ratios λ . In Fig. S1, we show the averaged values of slp , $\tilde{\Psi}_4$, $\tilde{\Psi}_6$ and $\tilde{\Psi}_8$ for each of the crystal phases.

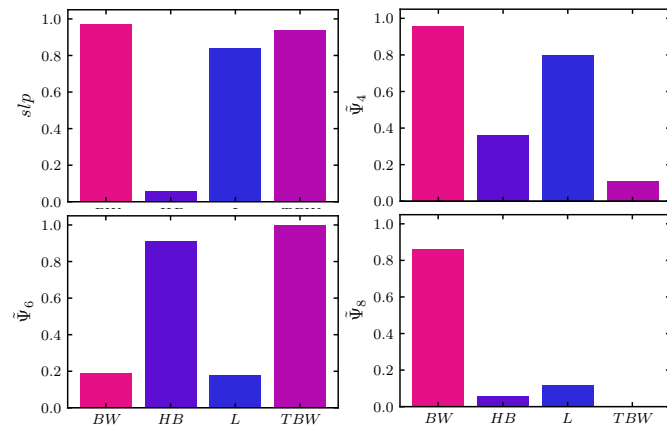


Fig. S1 Values of slp , $\tilde{\Psi}_4$, $\tilde{\Psi}_6$ and $\tilde{\Psi}_8$ for each crystal phase identified, namely brick-wall (BW), herringbone (HB), ladder-like (L) and tilted brick-wall (TBW).

3 State diagrams of triblock colloids in the colloid number density - depletant reservoir packing fraction representation

In Fig. S2(a,b), we present the state diagrams of triblock colloids with varying aspect ratio λ in the colloidal number density $\rho = N_c\sigma^2/A$ - depletant reservoir packing fraction η representation for two different depletant-to-colloid size ratios $q = \sigma_d/\sigma_{PS}$. In addition, regions where the second most prominent structure with a crystal fraction $N_x/N_c \geq 0.03$ corresponds to herringbone or tilted brick-wall are indicated with dark and light blue dashed rectangles, respectively. This analysis allows us to determine the maximum fraction of crystalline structures for each η , as reported in Fig. 4(a,b) of the main manuscript. Furthermore, disordered phases are colored according to their fractal dimension d_f , with lower values for large depletant reservoir packing fractions, corresponding to percolating networks.

In Fig. S3, we show the state diagram of triblock colloids with an aspect ratio $\lambda = 1.52$ in the colloidal number density $\rho = N_c\sigma^2/A$ - depletant reservoir packing fraction η representation for three different depletant-to-colloid size ratios $q = 0.05$, $q = 0.075$, and $q = 0.1$. The regions where the second most prominent structure corresponds to herringbone or tilted brick-wall are highlighted with dashed rectangles, respectively. This data is used to extract the maximum fraction of crystal for each depletant reservoir pack-

^a Soft Condensed Matter & Biophysics, Debye Institute for Nanomaterials Science, Utrecht University, Princetoonplein 1, 3584 CC Utrecht, The Netherlands; ^b International Institute for Sustainability with Knotted Chiral Meta Matter (WPI-SKCM²), Hiroshima University, 1-3-1 Kagamiyama, Higashi-Hiroshima, Hiroshima 739-8526, Japan; E-mails: fabrizio.camerin@gmail.com, s.marinaguilar@uu.nl, m.dijkstra@uu.nl

* These authors contributed equally to this work

ing fraction η and depletant-to-colloid size ratio q as shown in Fig. 4(c).

4 Effect of particle shape and interactions on the state diagram of anisotropic triblock colloids

To investigate the effect of particle shape and interactions on the state behavior, we adjust the degree of roughness and assign varying surface charges to different regions of the colloids. Specifically, we focus on an aspect ratio of $\lambda = 1.52$ and depletant-to-colloid size ratio $q = 0.05$, where we observe that under certain conditions of depletion interaction, the system nucleates into a brick-wall phase. We begin by examining the effect of surface charge heterogeneity associated with the two different materials. To do so, we reverse the surface charge between the tips and the center, essentially mimicking a triblock colloid composed of PS in the center and TPM at the tips. Hence, the centers of the triblock particle exhibit a stronger attraction than the tips. In Figure S4(b) we show the phase diagram in the colloid number density $\rho = N_c \sigma^2 / A$ - depletant reservoir packing fraction η representation. This state diagram is to be compared with Figure S4(a), which represents the "original" state diagram reported for the same conditions in the main text. As observed, reversing the surface charge impedes the nucleation of crystalline phases as the particles primarily interact center-to-center, resulting only in a disordered phase. Hence, we note the significance of having a stronger charge located at the center of the particle to obtain brick-wall and herringbone structures at $\lambda = 1.52$. Additionally, we study the case where all beads of the colloids interact with the same interaction potential, mimicking particles composed of only one material, in particular of PS. As shown in Figure S4(c), a brick-wall phase is still observed, albeit at slightly lower η .

Finally, we investigate how the roughness of individual particles affects their assembly by changing the number of beads used to tessellate the PS and TPM spheres. In Figure S4(d), we show the phase diagram of triblock colloids with a size ratio of $\lambda = 1.52$ and $N = 375$ beads used to tessellate each particle, resulting in a bead surface density of $\rho_b \sigma^2 = 2.28$. We notice a shift in the depletant concentration at which brick-wall structures emerge, as anticipated, given that a different number of beads affects the overall depth of the potential.

5 Nucleation

To investigate the nucleation behavior of the phases under examination, we conduct multiple simulation runs, allowing us to study various nucleation pathways for the same set of parameters. In particular, we focus on the aspect ratio $\lambda = 1.52$ and depletant-to-colloid size ratios $q = 0.05$ and $q = 0.075$, which yield the highest fraction of particles in a crystalline environment. In Fig. 5 of the main manuscript, we present one of the simulation runs corresponding to $q = 0.075$ and $\eta = 0.8$. Here, we report an additional simulation with the same parameters in Fig. S5. Comparing the two simulations, we observe analogous nucleation behavior. Initially, a small crystallite emerges, serving as a seed for the alignment of the surrounding particles, leading to the growth of a larger crystal grain. This progressive increase in the size of

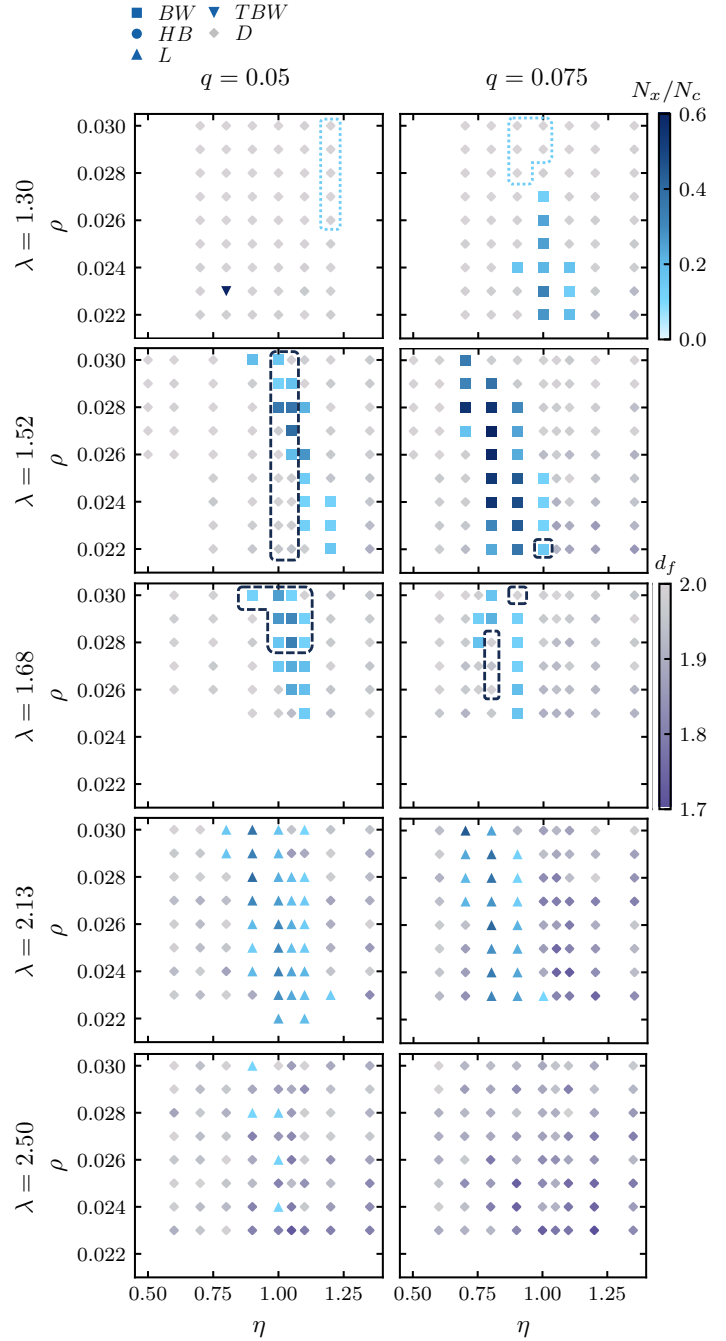


Fig. S2 State diagrams of triblock colloids with varying aspect ratio λ in the colloid number density $\rho = N_c \sigma^2 / A$ - depletant reservoir packing fraction η representation for depletant-to-colloid size ratio (left) $q = 0.05$ and (right) $q = 0.075$. Five different phases are identified, namely brick-wall (BW) (squares), herringbone (HB) (circles), ladder-like (L) (triangles), tilted brick-wall (TBW) (triangles down) and disordered (D) (diamonds) structures. For each state point, the most prevalent phase is reported. The symbols corresponding to crystal phases are colored according to the maximum crystal fraction N_x / N_c , following the color scale displayed at the upper part of the Figure. Symbols of the disordered phase are colored according to the value of their fractal dimension d_f , following the color scale located at the middle of the figure. Regions where HB occurs in less than 3% are marked with dark blue dashed rectangles, while TBW regions are delineated by light blue dashed rectangles.

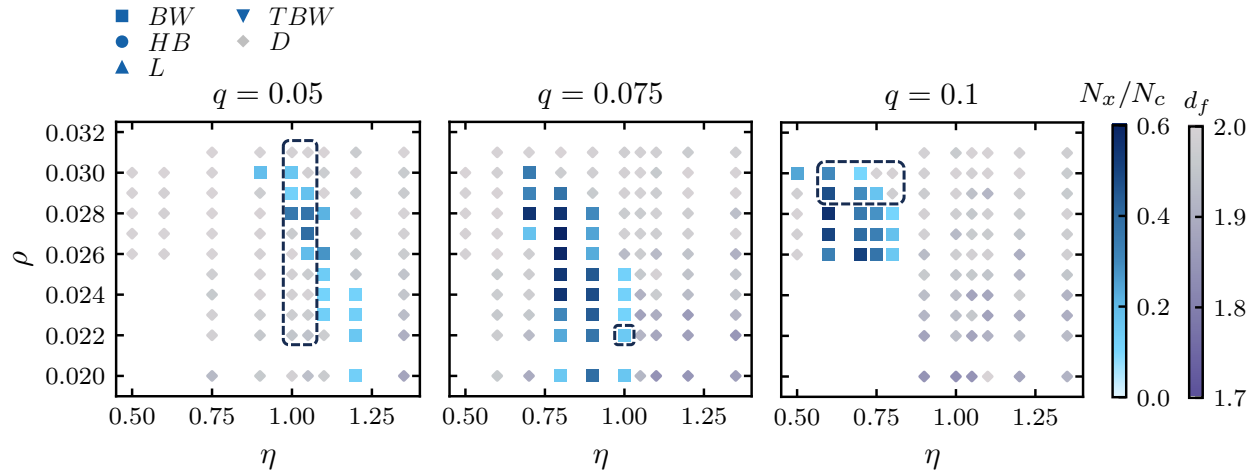


Fig. S3 State diagrams of triblock colloids with varying aspect ratio $\lambda = 1.52$ in the colloid number density $\rho = N_c \sigma^2 / A$ - depletant reservoir packing fraction η representation for depletant-to-colloid size ratio $q = 0.05, 0.075$, and 0.1 (from left to right). Five different phases are identified, namely brick-wall (BW) (squares), herringbone (HB) (circles), ladder-like (L) (triangles), tilted brick-wall (TBW) (triangles down) and disordered (D) (diamonds) structures. For each state point, the most prevalent phase is reported. Except for the disordered phase, symbols are assigned colors according to the maximum crystal fraction N_x/N_c , following the color scale displayed in the Figure. Symbols for the disordered phase are colored according to their fractal dimension d_f based on the color scale also displayed in the Figure. Regions where HB occurs in less than 3% are marked with dark blue dashed rectangles.

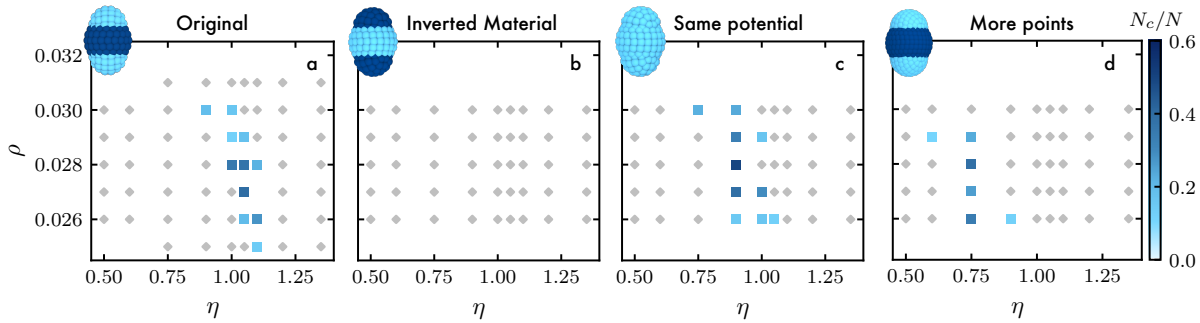


Fig. S4 State diagrams of triblock colloids with fixed aspect ratio $\lambda = 1.52$ and depletant-to-colloid size ratio $q = 0.05$ in the colloid number density $\rho = N_c \sigma^2 / A$ - depletant reservoir packing fraction η representation. Two different phases are identified, namely brick-wall shown with squares and disordered structures with diamonds. Panel (a) represents the model used in the main text with $N = 197$ number of beads per particle, (b) same conditions of number of beads per particle as in (a) but with surface charges reversed between center and tips, in (c) all beads interacting through the same potential corresponding to the tips of the original model, and (d) same conditions as in (a) but with $N = 375$ beads per triblock particle.

the crystal grain over time is evident from the time evolution of the fraction of particles in the largest crystal grain and the corresponding principal component, as shown in Fig. S5(b) and (c).

We extend our investigation to the nucleation of a system with $q = 0.05$, as illustrated in Fig. S6. Once again, we observe a similar behavior, with the formation of crystal grains that, after 40% of the total simulation time, merge leading to the formation of a larger crystal structure. This phenomenon is captured by a steeper increase in the fraction of particles in the largest crystal grain and the corresponding first principal component.

Finally, we also identify the seed for the herringbone phase, as shown in Fig. S7.

6 Disordered phases

In Fig. S8, we present representative simulation snapshots showing the different phases obtained for triblock colloids with an aspect ratio of $\lambda = 2.13$ for a depletant-to-colloid size ratio of

$q = 0.075$, a colloid number density of $\rho = N_c \sigma^2 / A = 0.024$, and varying depletant reservoir packing fractions η . Initially, at low η , the colloids exhibit a liquid-like behavior, before forming crystal grains and percolating network structures as η increases. Upon reaching the highest investigated η value, no crystalline order is observed, and the overall structure resembles that of a percolating gel.

In Fig. S2 and Fig. S3, we color the disordered phases according to their fractal dimension d_f . We observe that percolating systems exhibit a $d_f < 1.9$ and are primarily found at high depletant reservoir packing fractions.

7 3D Structures

In Fig. S9, we present representative simulation snapshots of the three-dimensional candidate crystal structures obtained using the floppy box Monte Carlo algorithm, as described in the Methods section, for varying aspect ratios λ . Additionally, we provide

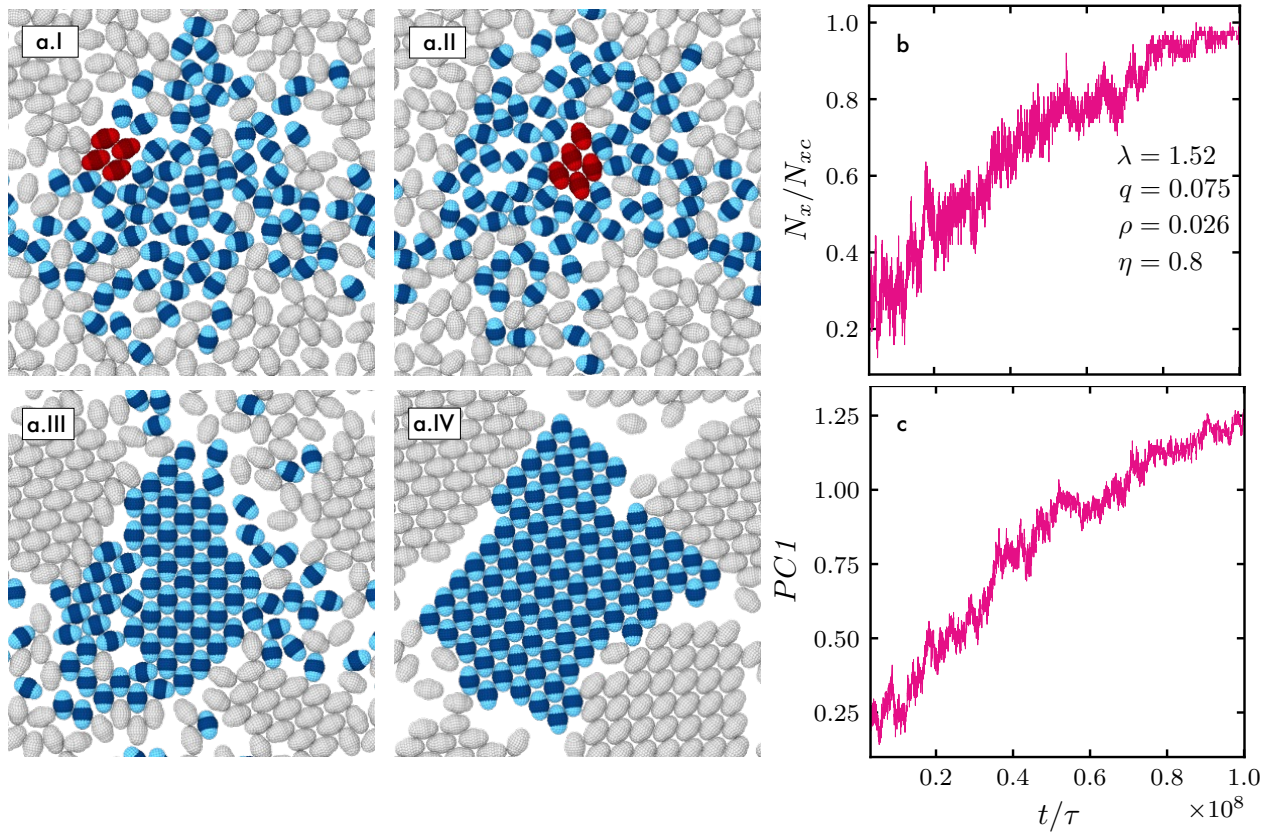


Fig. S5 (a.I-IV) Representative time-lapse simulation snapshots showing the formation of brick-wall crystals, (b) the fraction of brick-wall crystal N_x/N_{xc} as a function of simulation time t/τ , and (c) the first principal component (PC1) as a function of simulation time t/τ in a system of triblock colloids with aspect ratio $\lambda = 1.52$, depletant-to-colloid size ratio $q = 0.075$, depletant reservoir packing fraction $\eta = 0.8$ and colloid number density $\rho = N_c \sigma^2 / A = 0.026$ for the largest crystal grain identified in the last timestep of the simulation, reaching a size of N_{xc} particles. Red colloids highlight seeds of two grains that will be part of the largest crystal grain at the last timestep of the simulation. Grey colloids are not considered for the calculation of N_x/N_{xc} in (b) and for the PC1 in (c).

Supplementary Data 1, comprising the respective HTML files that facilitate the visualization of these configurations from different perspectives.

Notes and references

- 1 M. Liu, X. Zheng, V. Grebe, D. J. Pine and M. Weck, *Nature Materials*, 2020, **19**, 1354–1361.

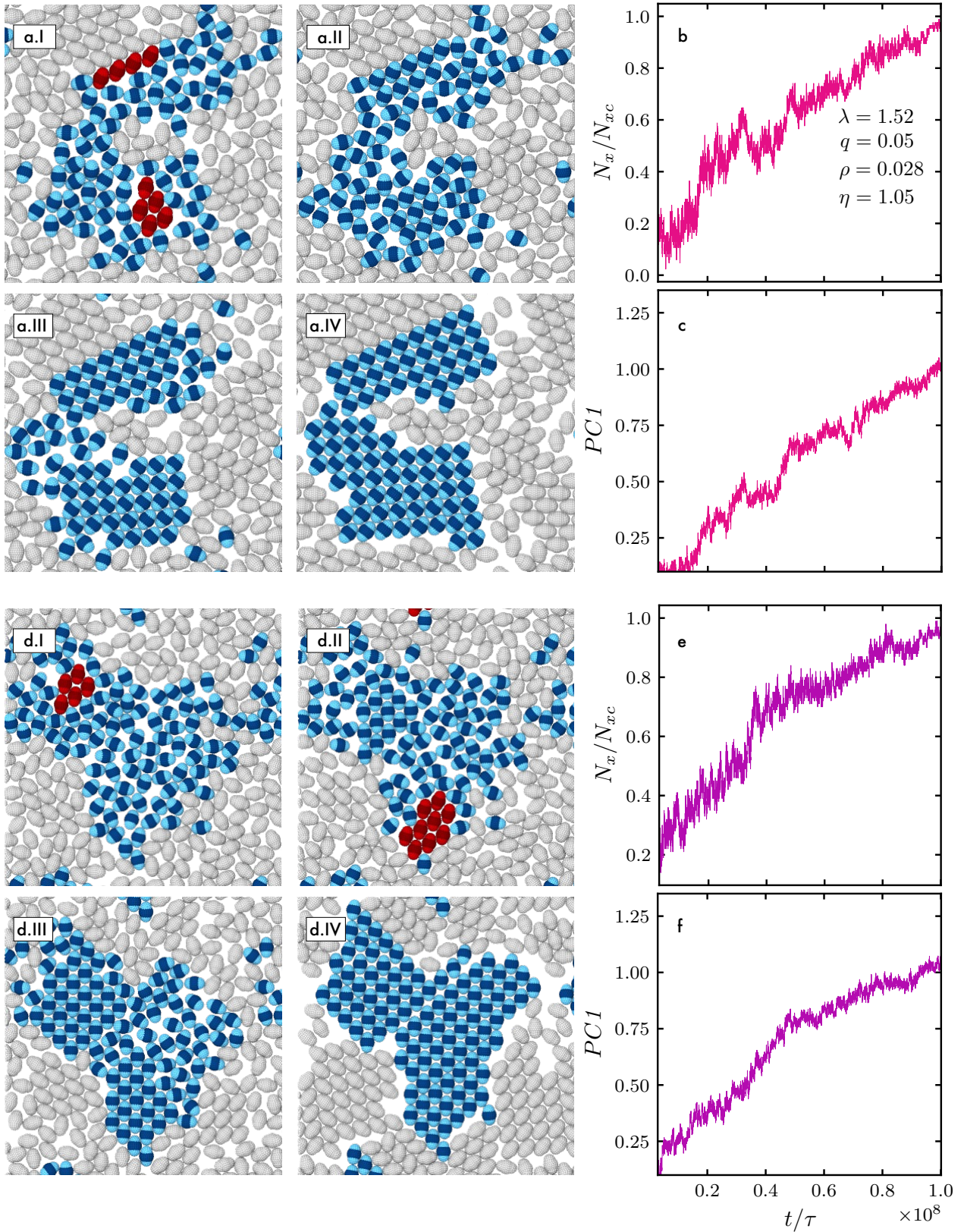


Fig. S6 (a.I-IV, d.I-IV) Representative time-lapse simulation snapshots showing the formation of brick-wall crystals, (b,e) the fraction of brick-wall crystal N_x/N_{xc} as a function of simulation time t/τ , and (c,f) the first principal component (PC1) as a function of simulation time t/τ for two independent simulation runs, respectively, in a system of triblock colloids with aspect ratio $\lambda = 1.52$, depletant-to-colloid size ratio $q = 0.05$, depletant reservoir packing fraction $\eta = 1.05$ and colloid number density of $\rho = N_c \sigma^2 / A = 0.028$ for the largest crystal grain identified in the last timestep of the simulation, reaching a size of N_{xc} particles. Red colloids highlight the seeds that will be part of the largest crystal grain at the last timestep of the simulation. Grey colloids are not considered for the calculation of N_x/N_{xc} in (b,c) and for the PC1 in (e,f).

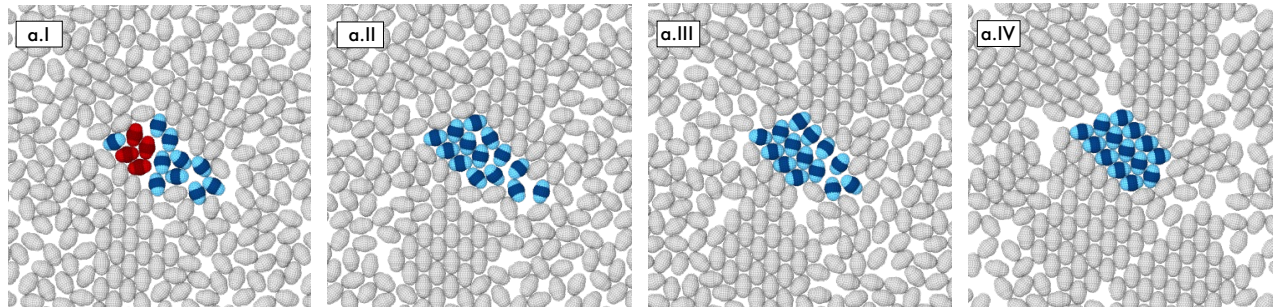


Fig. S7 (a.I-IV) Representative time-lapse simulation snapshots showing the formation of a herringbone crystal in a system of triblock colloids with aspect ratio $\lambda = 1.52$, depletant-to-colloid size ratio $q = 0.05$, depletant reservoir packing fraction $\eta = 1.05$ and colloid number density $\rho = N_c \sigma^2 / A = 0.028$ for the largest crystal grain identified in the last timestep of the simulation. Red colloids highlight the seed that will be part of the herringbone crystal in the last timestep of the simulation.

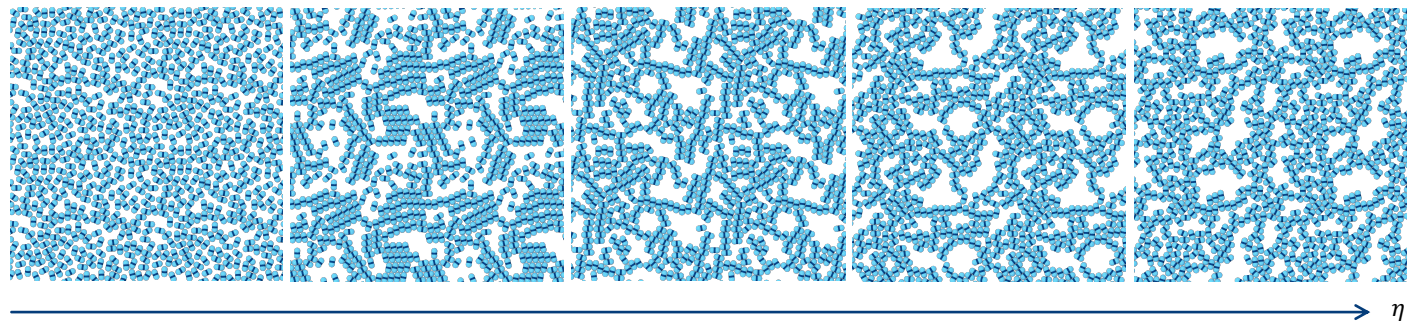


Fig. S8 Representative simulation snapshots showing a system of triblock colloids with aspect ratio $\lambda = 2.13$ for increasing depletant reservoir packing fraction $\eta = 0.60, 0.80, 0.90, 1.05$, and 1.2 (from left to right) with values of fractal dimension $df = 1.95, 1.75, 1.75, 1.74$ and 1.82 respectively, at a fixed depletant-to-colloid size ratio $q = 0.075$ and colloid number density $\rho = N_c \sigma^2 / A = 0.024$.

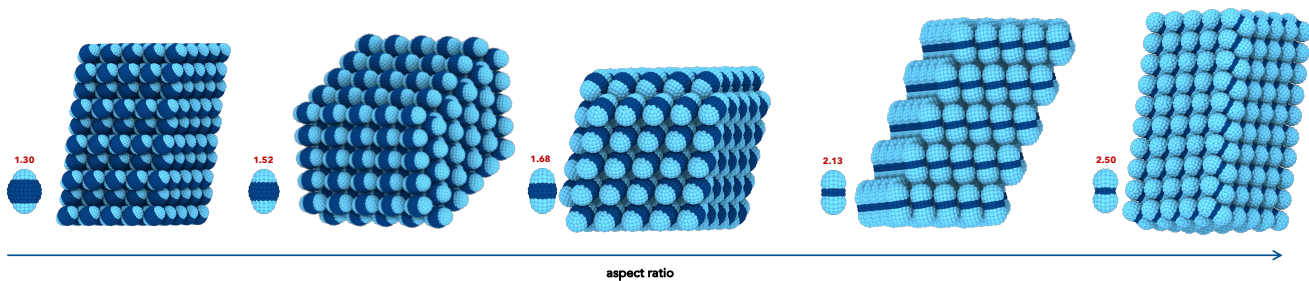


Fig. S9 Representative simulation snapshots obtained with the floppy box Monte Carlo algorithm showing 3D systems of triblock colloids with increasing aspect ratio $\lambda = 1.30, 1.52, 1.68, 2.13$ and 2.50 (from left to right).